

Rethinking Pan-sharpening: A New Training Process for Full-Resolution Generalization

Ran Zhang, Wenbo Xu, Fang Jiabin, Yang Qize, Liu Liu*

{2023212219, 2023170714, 2004fjb, 2023212231}@mail.hfut.edu.cn, liuliu@hfut.edu.cn

Xuanhua He, Li Xueheng, Ke Cao

University of Science and Technology of China

{hexuanhua, lixueheng, caoke200820}@mail.ustc.edu.cn

Jie Zhang

Hefei Institutes of Physical Science, Chinese Academy of Sciences

zhangjie@iim.ac.cn

Abstract

The field of pan-sharpening has recently seen a trend towards increasingly large and complex models, often trained on single, specific satellite datasets. This “one-dataset, one-model” approach leads to high computational overhead and impractical deployment. More critically, it overlooks a core challenge: poor generalization from reduced-resolution (RR) training to real-world full-resolution (FR) data. In response to this issue, we challenge this paradigm. We introduce a “multiple-in-one” training strategy, where a single, compact model is trained simultaneously on three distinct satellite datasets (WV2, WV3, and GF2). Our experiments show the primary benefit of this unified strategy is a significant and universal boost in FR generalization (QNR) across all tested models, directly addressing this overlooked problem. This paradigm also inherently solves the ‘one-model-per-dataset’ challenge, and we support it with a highly reproducible, dependency-free codebase for true usability. Finally, we propose PanTiny, a lightweight framework designed specifically for this new, robust paradigm. We demonstrate it achieves a superior performance-to-efficiency balance, proving that principled, simple and robust design is more effective than brute-force scaling in this practical setting. Our work advocates for a community-wide shift towards creating efficient, deployable, and truly generalizable models for pan-sharpening. The code is open-sourced at <https://github.com/Zirconium233/PanTiny>.

*Corresponding author.

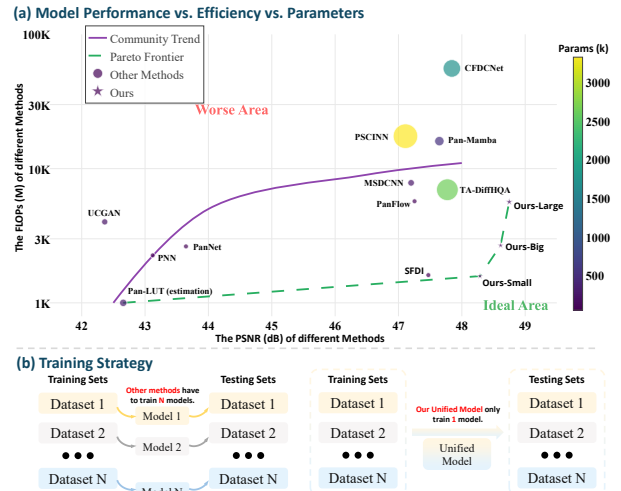


Figure 1. Our proposed PanTiny framework enables training a single, unified model on multiple datasets (WV2, WV3, GF2) simultaneously. This all-in-one approach achieves SOTA performance while maintaining a significantly smaller model size and lower computational cost compared to methods that require separate, specialized models for each dataset.

1. Introduction

Pan-sharpening, a fundamental image fusion task in remote sensing, aims to merge a high-resolution panchromatic (PAN) image with a lower-resolution multispectral (LRMS) image to generate a single high-resolution multispectral (HRMS) image [13, 18]. This fused image is crucial for numerous downstream applications [13, 18].

Early approaches were dominated by traditional methods [3, 5, 9, 12]. The advent of deep learning, particularly with models like PNN [13] and PanNet [18], revolutionized the field by learning complex mappings directly from data and significantly improving fusion quality.

However, the recent pursuit of higher performance has led to a research landscape heavily focused on *model architecture innovation*. This trend generally follows three main directions. First, some works attempt to solve cross-dataset generalization, developing complex features to bridge the significant domain gaps between satellites [21]. Second, a dominant trend is the adaptation of SOTA architectures from other vision fields to pan-sharpening, including porting State-Space Models (SSMs) like Pan-Mamba [8] and flow-based models [17]. Third, some models achieve high metrics through brute-force scaling, resulting in massive, complex architectures. For instance, CFDCNet [11] achieves high metrics but at the cost of an astounding 55G FLOPs.

While these approaches have pushed benchmarks, they share common drawbacks: they are almost all evaluated on reduced-resolution (RR) benchmarks, and they adhere to a “one-dataset, one-model” philosophy. We argue this focus on architectural novelty overlooks two more fundamental, practical challenges. First, the “one-dataset, one-model” paradigm is impractical. It requires training and maintaining separate, specialized models for each satellite sensor, complicating real-world deployment. Second, and most critically, the true, practical challenge is full-resolution (FR) generalization—the ability for a model trained on RR data to perform well on real-world, full-resolution images. This crucial aspect is largely unaddressed. Furthermore, as our supplementary material shows, the domain gaps between satellites are so large that *cross-dataset* generalization (the goal of [21]) is often futile, suggesting that joint training is a more pragmatic path forward.

In this work, we propose a comprehensive solution that challenges these norms by shifting the focus from *model architecture* to the *training process* and *practical efficiency*. First, we introduce a new “all-in-one” training paradigm, representing a novel process-level innovation. We are the first to demonstrate that a single model can be jointly trained on multiple heterogeneous datasets (WV2, WV3, GF2). The primary benefit is not maximizing RR metrics, but as we will show, dramatically and universally boosting FR generalization (Table 2) across all tested models.

Second, this paradigm inherently solves the deployment and usability problem. As illustrated in Figure 1, a single, compact model can now service three distinct datasets, replacing the cumbersome ‘one-model-per-dataset’ approach.

Finally, we demonstrate that principled, lightweight engineering is superior to brute-force scaling. We propose PanTiny, a lightweight model designed specifically for this

paradigm, and a universally powerful composite loss function. Our PanTiny model, benefiting from these innovations, achieves a superior performance-to-efficiency balance, outperforming most larger, specialized models [11]. Critically, unlike models such as Pan-Mamba [8] or CFDCNet [11], PanTiny uses only standard, universally available operators, making it dependency-free, easy to reproduce, and highly practical for deployment.

Our contributions are threefold:

- We propose and validate a new “all-in-one” training paradigm, a process-level innovation that shifts the field’s focus from model-centric design and demonstrably boosts generalization on full-resolution data.
- We address the ‘one-model-per-dataset’ problem by training a single, unified model for multiple datasets, significantly improving deployment efficiency and usability, as illustrated in Figure 1.
- We propose PanTiny, a lightweight yet powerful model, and a universal composite loss, which together prove that principled, efficient design—which is also dependency-free and easy to reproduce—can surpass brute-force scaling within this new paradigm.

2. Related Work

2.1. Traditional and Early Deep Learning Methods

Traditional pan-sharpening methods include Component Substitution (CS) [3, 5], which enhances spatial detail but risks spectral distortion, and Multi-Resolution Analysis (MRA) [9, 12], which better preserves spectral information but can add spatial artifacts. Deep learning (DL) methods later surpassed these, with pioneering works like PNN [13] using a simple CNN. PanNet [18] improved upon this by working in the high-frequency domain, and subsequent models like MSDCNN [19] explored multi-scale features to enhance fusion quality.

2.2. SOTA Architectural Innovation

Recent work is dominated by model-centric innovation, often adapting SOTA architectures from other vision fields. This includes porting State-Space Models (e.g., Pan-Mamba [8]), flow-based models (e.g., PanFlow [17]), and invertible neural networks (e.g., PSCINN [15]). Another trend is brute-force scaling, exemplified by CFDCNet [11], which achieves high metrics but at an enormous computational cost (55G FLOPs).

2.3. Data Generalization Paradigms

Research on data generalization is also prevalent. Most methods follow a “one-dataset, one-model” philosophy. While some attempt *cross-dataset* generalization (e.g., train on A, test on B) by learning domain-irrelevant features [21], this approach often fails due to large domain gaps between

sensors. The concept of an “all-in-one” model, trained jointly on multiple datasets, remains largely unexplored. Our work addresses this gap, proposing a unified paradigm to solve the deployment problem and, critically, to improve *full-resolution generalization*—a practical challenge largely unaddressed by the community.

3. Methodology

Our proposed method, PanTiny, is built on the principles of efficiency, simplicity, and empirical validation, designed specifically to be robust and effective within our “all-in-one” training paradigm. As our new focus is on multi-domain training, we deliberately avoid overly complex operators that, as we will show (Table 7), are prone to overfitting. We instead focus on a clean, effective architecture where each component’s inclusion is justified by extensive experiments. The overall architecture, shown in Figure 2, features a single-encoder design, a Transformer-based body for feature processing, and a simple convolutional refinement head.

3.1. Overall Architecture

3.1.1. Patch Embedding and Encoding

Unlike many methods that use separate encoders, we adopt an efficient single-encoder architecture. The upsampled MS image (bms) is first passed through an OverlapPatchEmbed layer (a 3x3 convolution) to extract initial features. These features are then processed by a shallow set of Transformer blocks (self.encoder in our implementation).

3.1.2. Feature Fusion Module

Following the initial encoding, the PAN image is integrated directly in the feature space via our fusion module. Our investigation into fusion mechanisms revealed a surprising insight: **in the multi-dataset “all-in-one” context, simplicity triumphs over complexity**. We found that complex, specialized fusion strategies like the multi-layer “deepfusion” block [8] (Table 7) **degraded performance, suggesting overfitting** to dataset-specific artifacts. This “specialized knowledge” fails when the model must perform across multiple domains. Therefore, we adopt a simple but highly effective Enhanced Conv” block (two consecutive 3x3 convolutional layers), which our ablations (Table 7) proved to be the most robust.

3.1.3. Deep Feature Processing and Refinement

The fused features are then processed by the main body of the network (self.refinement in code), which consists of a deeper stack of standard Transformer blocks for effective long-range dependency modeling. For the final reconstruction, we again prioritize simplicity. Our experiments (Table 8) confirmed that a **single convolutional layer** was optimal, while more elaborate refinement modules offered no

significant benefit and unnecessarily increased model size.

3.2. Transformer Block

While the overall structure is inspired by the original Transformer, our implementation uses a Pre-LayerNorm (Pre-LN) configuration for improved training stability. For an input feature map X_{l-1} , the output X_l of a single Transformer block is computed as:

$$X'_l = \text{CA}(\text{LN}(X_{l-1})) + X_{l-1} \quad (1)$$

$$X_l = \text{GDFN}(\text{LN}(X'_l)) + X'_l \quad (2)$$

where LN denotes Layer Normalization, CA is our Channel Attention module, and GDFN is a Gated-DConv Feed-Forward Network.

Channel Attention (CA). The CA module captures global context by performing self-attention across channel dimensions. Given an input $X \in \mathbb{R}^{B \times C \times H \times W}$, we first generate the query (Q), key (K), and value (V) projections via depth-wise convolutions. The attention map is then computed as:

$$\text{Attention}(Q, K, V) = \text{Softmax}((Q_n K_n^T) \cdot \tau) V_n \quad (3)$$

where Q_n and K_n are L2-normalized query and key tensors, and τ is a learnable temperature parameter that scales the attention map. This design avoids the standard scaling by feature dimension, instead allowing the network to learn the optimal attention scaling.

Gated-DConv Feed-Forward Network (GDFN). To enhance feature representation efficiently, we employ a gated feed-forward network. An input tensor is first projected to a higher-dimensional space and then split into two parallel paths, X_1 and X_2 . The output is computed as:

$$\text{GDFN}(X) = \text{Conv}_{\text{out}}(\text{GELU}(\text{DWConv}(X_1)) \odot \text{DWConv}(X_2)) \quad (4)$$

where \odot denotes element-wise multiplication. This gating mechanism allows for more dynamic and expressive feature transformations compared to a standard FFN.

3.3. Loss Function

The choice of loss function is critical for training high-performance restoration models. While many prior works rely solely on the L1 loss, our empirical study showed that a composite loss function yields substantially better results. Our total loss L_{total} is a weighted sum of three components, applied to the model’s output O and the ground truth G :

$$L_{total} = \lambda_1 L_1 + \lambda_2 L_{SSIM} + \lambda_3 L_{Focal} \quad (5)$$

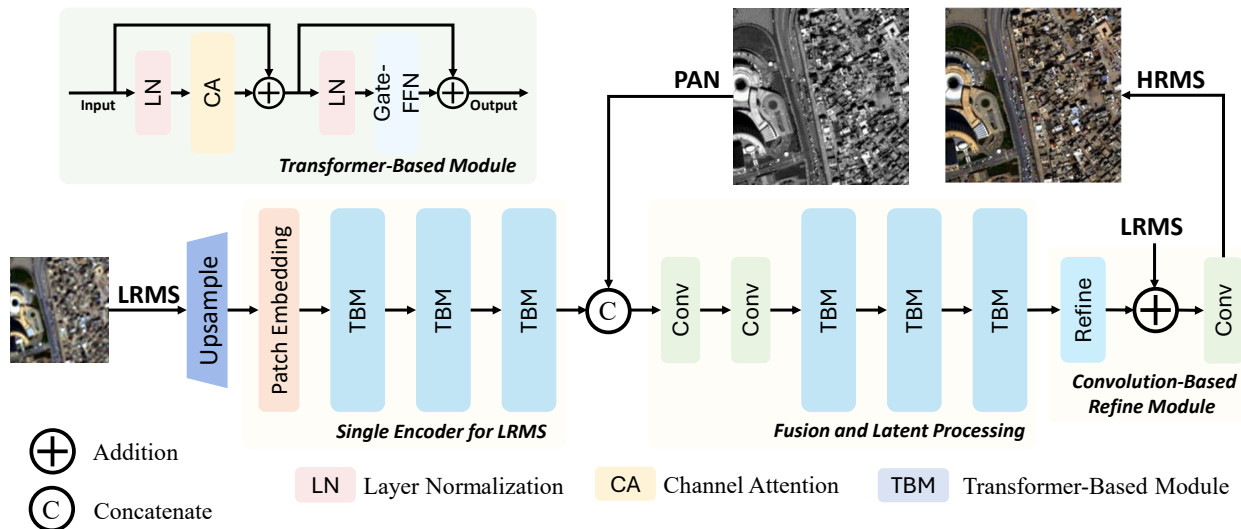


Figure 2. The overall architecture of our proposed PanTiny framework. It consists of a single lightweight convolutional encoder for the MS input, a simple yet effective fusion module to integrate PAN information, a body of standard Transformer blocks for deep feature interaction, and a final convolutional layer for refinement.

Model	Params(K)	FLOPs(G)	WV2			WV3			GF2		
			PSNR \uparrow	SSIM \uparrow	SAM \downarrow	PSNR \uparrow	SSIM \uparrow	SAM \downarrow	PSNR \uparrow	SSIM \uparrow	SAM \downarrow
<i>Traditional Methods</i>											
Brovey [7]	-	-	35.86	0.9216	0.0403	22.50	0.5466	0.1159	37.79	0.9026	0.0218
IHS [3]	-	-	35.29	0.9027	0.0461	22.55	0.5354	0.1266	38.17	0.9100	0.0243
SFIM [12]	-	-	34.12	0.8975	0.0439	21.82	0.5457	0.1208	36.90	0.8882	0.0318
GS [10]	-	-	35.63	0.9176	0.0423	22.56	0.5470	0.1217	37.22	0.9034	0.0309
<i>Deep Learning Methods (All-in-One Training)</i>											
PNN [13]	68.9	2.26	39.82	0.9540	0.0282	29.49	0.9005	0.0861	43.14	0.9667	0.0178
PanNet [18]	80.3	2.63	38.98	0.9468	0.0301	29.12	0.8927	0.0935	43.26	0.9668	0.0176
MSDCNN [19]	239.0	7.83	40.31	0.9580	0.0267	29.63	0.9033	0.0833	43.21	0.9671	0.0176
PanFlow [17]	87.3	2.86	41.11	0.9645	0.0243	30.04	0.9106	0.0799	46.36	0.9825	0.0125
PSCINN [15]	3321.5	108.84	35.60	0.8967	0.0336	22.61	0.5538	0.1115	42.69	0.9616	0.0181
Pan-Mamba [8]	488.8	16.02	41.39	0.9663	0.0236	30.17	0.9174	0.0779	43.98	0.9725	0.0164
CFDCNet [11]	1700.8	55.73	41.54	0.9667	0.0233	<u>30.42</u>	0.9155	0.0775	47.76	<u>0.9866</u>	0.0107
PanTiny (Small)	48.3	1.58	<u>41.62</u>	<u>0.9685</u>	<u>0.0230</u>	30.38	<u>0.9216</u>	<u>0.0768</u>	<u>48.16</u>	0.9884	<u>0.0099</u>
PanTiny (Big)	81.7	2.68	41.85	0.9696	0.0224	30.59	0.9238	0.0749	48.61	0.9894	0.0095

Table 1. Main quantitative comparison. All models are trained simultaneously on WV2, WV3, and GF2 datasets and evaluated on each using a single model. Our PanTiny (Big) achieves the best performance across all datasets. ‘-’ indicates a traditional, non-learning based approach. Best results are in **bold**, second-best are underlined.

- **L1 Loss:** We use the Charbonnier loss [4], a differentiable variant of the L1 norm that is less sensitive to outliers. For

a batch of B images with N pixels each, it is defined as:

$$L_1 = \frac{1}{B \cdot N} \sum_{i=1}^{B \cdot N} \sqrt{(O_i - G_i)^2 + \epsilon^2} \quad (6)$$

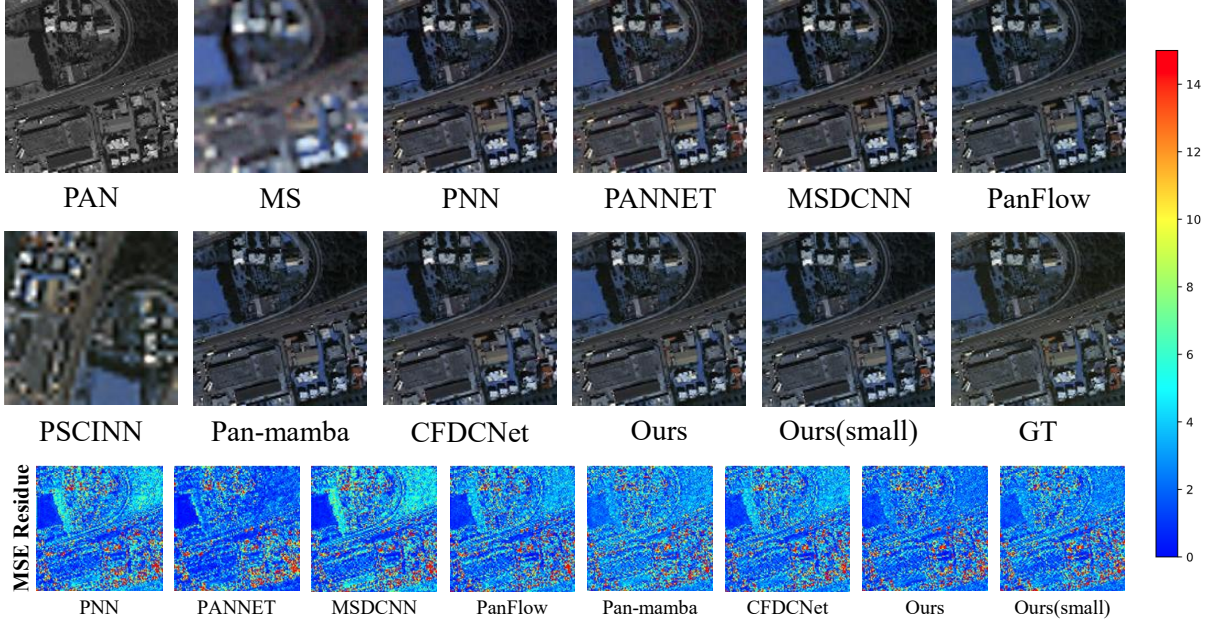


Figure 3. Quality comparison across SOTA methods on WV3 dataset. Refer to supplementary materials for more results.

Model	QNR \uparrow	
	Separate	All-in-One
MSDCNN [19]	0.7683	<u>0.8898</u>
PanNet [18]	0.7684	0.8726
PNN [13]	0.7527	0.8844
PSCINN [15]	0.7904	0.8849
PanTiny (Small)	0.7827	0.8751
PanTiny (Big)	0.7985	0.8793
PanFlow [17]	0.7910	0.8900

Table 2. Generalization on WV2 full-resolution data. All-in-one training significantly boosts the QNR metric for all models.

where ϵ is a small constant (e.g., 10^{-6}) for numerical stability.

- **SSIM Loss:** To preserve perceptual quality and high-frequency structural details, we incorporate the Structural Similarity (SSIM) loss [16]. The SSIM index between

two image patches o and g is:

$$\text{SSIM}(o, g) = \frac{(2\mu_o\mu_g + C_1)(2\sigma_{og} + C_2)}{(\mu_o^2 + \mu_g^2 + C_1)(\sigma_o^2 + \sigma_g^2 + C_2)} \quad (7)$$

where μ and σ represent the mean and variance, and C_1, C_2 are stabilizing constants. The final loss is computed as $L_{SSIM} = 1 - \text{SSIM}(O, G)$, averaged over all patches. Our ablations in Table 6 clearly show its importance.

- **Focal-Inspired Regression Loss:** Inspired by the *principle* of focal loss in classification, we adapt its core idea to regression to prioritize “hard” pixels. We term this L_{Focal} . Let $d_i = |O_i - G_i|$ be the absolute error for a given pixel i (assumed to be in the $[0, 1]$ normalized range). Our loss is formulated as:

$$L_{Focal} = \frac{1}{B \cdot N} \sum_{i=1}^{B \cdot N} \frac{(255 \cdot d_i)^{r_1}}{255} \cdot d_i \quad (8)$$

where the constant 255 scales the normalized error back to the 8-bit dynamic range before applying the exponent, stabilizing the gradient. **In our experiments, we use a focusing parameter $r_1 = 1.1$.** This formulation acts as a non-linear weighting function: by setting $r_1 > 1.0$, pixels with larger errors (hard” pixels) are polynomially up-

weighted, compelling the model to focus on challenging details, similar in effect to a high-order L_p loss.

Through extensive experiments (detailed in Table 6 and our supplementary material), we determined the optimal weights to be $\lambda_1 = 1.5$, $\lambda_2 = 4.0$, and $\lambda_3 = 1.5$, which consistently delivered the best performance.

4. Experiments

4.1. Setup

Datasets. We conduct experiments on three public datasets: WorldView-2 (WV2), WorldView-3 (WV3), and GaoFen-2 (GF2). **It is a standard community practice [13, 18] to pre-process the 8-band WV2 and WV3 data to 4-bands (R, G, B, NIR) to match GF2. We follow this standard, using the 4-band versions to ensure fair comparison and enable our “all-in-one” joint training. For our primary “all-in-one” experiments, we combine the training sets of all three. We follow standard protocols for evaluation, using both reduced-resolution and full-resolution test sets.**

Evaluation Metrics. We provide a comprehensive evaluation using both reference and no-reference metrics. For reduced-resolution evaluation, we use Peak Signal-to-Noise Ratio (PSNR), Structural Similarity (SSIM) [16], Spectral Angle Mapper (SAM) [20], and ERGAS [14]. For full-resolution evaluation, we use the no-reference metrics D_λ , D_s , and QNR [1].

Implementation Details. Our framework is implemented in PyTorch. All models are trained on a single NVIDIA RTX 4090 GPU. We use the ADAM optimizer with a learning rate of 5×10^{-4} and betas of (0.9, 0.999). A cosine annealing scheduler adjusts the learning rate over 500 epochs with a batch size of 16.

4.2. The “All-in-One” Training Paradigm

Our experimental evaluation is first designed to validate our core thesis: that the “all-in-one” training paradigm is a more robust and effective method for developing generalizable pan-sharpening models, solving the key challenges of FR generalization and deployment practicality.

4.2.1. Limitations of Traditional Paradigms

We first analyze the impact of our “all-in-one” paradigm on the traditional reduced-resolution (RR) benchmarks, as shown in Table 3. The results are mixed: compared to “Separate” models that are highly specialized (overfitted) to a single dataset, the “All-in-One” models (e.g., Pan-Mamba [8] and PSCINN [15]) show a significant performance drop on RR metrics. This highlights that the domain gaps between satellites are severe, and models must balance conflicting objectives. In contrast, our “PanTiny (Big)” model is remarkably robust, with only a minor drop on WV2/GF2 and almost no change on WV3. This demonstrates that sim-

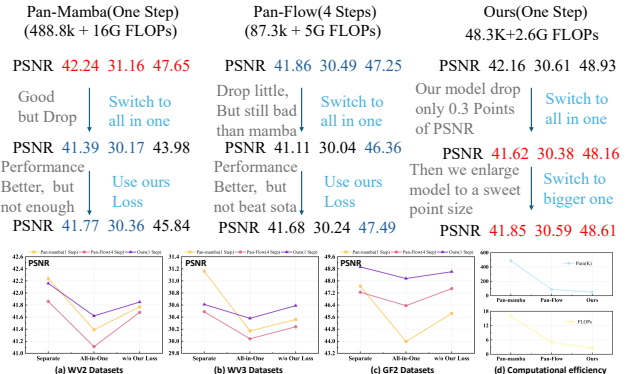


Figure 4. Performance trajectory of the ablation study. This figure illustrates the performance changes of different models under the “all-in-one” training paradigm.

ply chasing RR benchmark scores on a single dataset is not a robust strategy.

4.2.2. The True Value: Full-Resolution Generalization

The primary goal of pan-sharpening is real-world application, which requires generalizing from RR training to FR inference. Table 2 reveals the true, unambiguous value of our paradigm. For **all models tested**, switching from “Separate” to “All-in-One” training results in a **dramatic and universal improvement in the full-resolution QNR metric**. For instance, PanFlow’s [17] QNR score on WV2 jumps from 0.7910 to 0.8900, and MSDCNN’s [19] from 0.7683 to 0.8898. This is clear evidence that our paradigm trains models to be far more robust and generalizable to the real-world FR task. This, combined with the inherent benefit of deploying a single unified model (our Contribution 2), underscores the power of our proposed method.

4.3. PanTiny: An Efficient SOTA Model for the New Paradigm

Having established the “all-in-one” paradigm as a superior and more practical approach, we now benchmark models within this framework to validate our proposed PanTiny (Contribution 3).

4.3.1. Main Results on Multi-Dataset Training

Table 1 presents the main results. Our proposed PanTiny (Big) achieves SOTA performance across all three datasets, outperforming both classic and recent methods. Notably, it surpasses CFDCNet [11], a much larger model, on all metrics. PanTiny (Small) also achieves a highly competitive performance-to-efficiency balance. The results for PSCINN [15] highlight its instability in this multi-dataset setting, as it failed to complete training, which we consider a practical failure, further validating our robust design choice.

Model	Training	WV2			WV3			GF2		
		PSNR \uparrow	SSIM \uparrow	SAM \downarrow	PSNR \uparrow	SSIM \uparrow	SAM \downarrow	PSNR \uparrow	SSIM \uparrow	SAM \downarrow
Pan-Mamba [8]	All-in-One	41.39	0.9663	0.0236	30.17	0.9174	0.0779	43.98	0.9725	0.0164
	Separate	42.24	0.9729	0.0212	31.16	0.9299	0.0702	47.65	0.9894	0.0103
PNN [13]	All-in-One	39.82	0.9540	0.0282	29.49	0.9005	0.0861	43.14	0.9667	0.0178
	Separate	40.76	0.9624	0.0259	29.94	0.9121	0.0824	43.12	0.9704	<u>0.0172</u>
PanFlow [17]	All-in-One	41.11	0.9645	0.0243	30.04	0.9106	0.0799	46.36	0.9825	0.0125
	Separate	41.86	0.9712	0.0224	30.49	0.9221	0.0751	47.25	0.9884	0.0103
PSCINN [15]	All-in-One	35.60	0.8967	0.0336	22.61	0.5538	0.1115	42.69	0.9616	0.0181
	Separate	41.85	0.9703	0.0223	30.56	0.9230	0.0748	47.11	0.9878	0.0107
CFDCNet [11]	All-in-One	41.54	0.9667	0.0233	30.42	0.9155	0.0775	47.76	0.9866	0.0107
	Separate	42.24	0.9733	0.0209	31.24	0.9327	0.0694	47.84	0.9902	0.0097
Pan-LUT [2]	All-in-One	-	-	-	-	-	-	-	-	-
	Separate	39.84	0.9555	0.0286	28.82	0.8936	0.0935	42.66	0.9642	0.0189
Ours (PanTiny Big)	All-in-One	<u>41.85</u>	<u>0.9696</u>	<u>0.0224</u>	<u>30.59</u>	<u>0.9238</u>	<u>0.0749</u>	<u>48.61</u>	<u>0.9894</u>	<u>0.0095</u>
	Separate	42.16	0.9711	0.0217	30.61	0.9245	0.0747	48.93	0.9900	0.0092

Table 3. Performance comparison between “all-in-one” and “separate” dataset training. “Separate” results are from original papers. The performance gap highlights the generalization challenge for complex, specialized models.

Model	Params(K)	FLOPs(G)	WV2			WV3			GF2		
			PSNR \uparrow	SSIM \uparrow	SAM \downarrow	PSNR \uparrow	SSIM \uparrow	SAM \downarrow	PSNR \uparrow	SSIM \uparrow	SAM \downarrow
CFDCNet [11]	1700.8	55.73	42.50	0.9729	0.0205	31.11	0.9298	0.0707	49.07	0.9903	0.0091
Pan-Mamba [8]	488.8	16.02	41.77	0.9691	0.0226	30.36	0.9215	0.0769	45.84	0.9811	0.0134
PanFlow [17]	87.3	2.86	41.68	0.9688	0.0229	30.24	0.9197	0.0785	47.49	0.9865	0.0109
MSDCNN [19]	239.0	7.83	41.46	0.9669	0.0236	30.18	0.9189	0.0786	44.09	0.9730	0.0161
PNN [13]	68.9	2.26	40.84	0.9635	0.0256	29.82	0.9128	0.0834	43.40	0.9688	0.0173
PanNet [18]	80.3	2.63	40.79	0.9620	0.0256	29.82	0.9106	0.0841	43.76	0.9705	0.0167
DeepPNN (ours)	271.1	8.88	41.89	0.9700	0.0224	30.43	0.9228	0.0759	47.45	0.9869	0.0109
ResAtten (ours)	263.0	8.62	<u>41.97</u>	<u>0.9702</u>	<u>0.0222</u>	30.40	0.9223	0.0759	47.14	0.9856	0.0113
PanTiny (Big)	81.7	2.68	41.85	0.9696	0.0224	<u>30.59</u>	<u>0.9238</u>	<u>0.0749</u>	<u>48.61</u>	<u>0.9894</u>	<u>0.0095</u>
PanTiny (Small)	48.3	1.58	41.62	0.9685	0.0230	30.38	0.9216	0.0768	48.16	0.9884	0.0099

Table 4. Model architecture ablation under our unified loss. Our proposed loss benefits all models, but our architecture remains highly competitive. Performance gains over original reported results are due to our improved training strategy.

Model	Params (K)	WV2		WV3		GF2	
		PSNR	SSIM	PSNR	SSIM	PSNR	SSIM
PanTiny (Small)	48.3	41.62	0.9685	30.38	0.9216	48.16	0.9884
PanTiny (Big)	81.7	41.85	0.9696	30.59	0.9238	48.61	0.9894
PanTiny (Large Body)	172.4	<u>42.06</u>	<u>0.9708</u>	<u>30.67</u>	<u>0.9248</u>	<u>48.75</u>	<u>0.9896</u>
PanTiny (Huge Body)	195.9	42.12	0.9711	30.74	0.9258	48.85	0.9898

Table 5. Ablation on model size. Brute-force scaling yields diminishing returns compared to our efficient ‘Big’ design.

4.3.2. Architectural Design and Efficiency

PanTiny’s SOTA performance is achieved with superior efficiency. As shown in Table 1, its 81.7K parameters and 2.68G FLOPs are orders of magnitude smaller than heavyweight competitors like CFDCNet (1700.8K params,

55.73G FLOPs) [11]. We further explore scaling in Table 5. By expanding our model to a ‘Huge’ version (195.9K params), we can nearly match CFDCNet’s best-in-class performance on GF2 (48.85 vs 49.07 PSNR) at less than 12% of its parameter count. This reinforces our core argument that principled, efficient engineering surpasses brute-force scaling. Critically, PanTiny’s practical efficiency also lies in its **reproducibility**. Unlike Pan-Mamba [8] or CFDCNet [11] which may rely on specialized CUDA kernels or dependencies, PanTiny is built with standard PyTorch operators, ensuring it is easy to deploy and validate.

Loss Combination (L1, SSIM, Focal)	WV2			WV3			GF2		
	PSNR \uparrow	SSIM \uparrow	SAM \downarrow	PSNR \uparrow	SSIM \uparrow	SAM \downarrow	PSNR \uparrow	SSIM \uparrow	SAM \downarrow
L1 only (1.0, 0, 0)	39.77	0.9532	0.0285	29.19	0.8939	0.0953	45.42	0.9782	0.0141
SSIM only (0, 1.0, 0)	40.82	0.9648	0.0254	29.91	0.9158	0.0816	47.21	0.9865	0.0111
Focal only (0, 0, 1.0)	39.87	0.9545	0.0281	29.18	0.8937	0.0933	44.80	0.9757	0.0150
Balanced (0.8, 0.5, 0.4)	41.00	0.9640	0.0248	29.99	0.9128	0.0832	47.38	0.9859	0.0110
Equal (1.0, 1.0, 1.0)	41.28	0.9659	0.0240	30.17	0.9170	0.0791	47.68	0.9869	0.0105
High Weight (3.0, 3.0, 3.0)	41.68	0.9683	0.0229	30.49	0.9214	0.0762	48.30	<u>0.9885</u>	<u>0.0099</u>
SSIM Focus (0.5, 8.0, 0.5)	<u>41.68</u>	0.9694	0.0228	30.45	0.9233	0.0760	48.17	0.9887	0.0100
Ours (1.5, 4.0, 1.5)	41.70	<u>0.9689</u>	0.0228	<u>30.46</u>	<u>0.9225</u>	<u>0.0761</u>	<u>48.29</u>	0.9887	0.0098

Table 6. Ablation study on loss function components and weights using our PanTiny model. Our proposed combination (1.5, 4.0, 1.5) provides the best overall performance.

4.4. Ablation Studies and Further Analysis

We validate the specific design choices for our loss function and the PanTiny architecture.

4.4.1. PanTiny’s Architectural Ablations

We now validate the internal design choices of PanTiny to demonstrate that its simplicity is a principled and effective strategy. We conducted detailed ablations on its core fusion and refinement components.

Fusion Module: The fusion mechanism is critical for integrating PAN and MS information. As shown in Table 7, we tested several alternatives. A simple “1x1 Conv” provides a strong baseline, but our proposed “Enhanced Conv” (a 2-layer Conv) achieves the best overall performance. Notably, we also tested the complex “DeepFusion” module from Pan-Mamba [8]. This module, while effective in its original single-dataset setting, performs poorly here. This result strongly suggests that complex, specialized modules tend to overfit to dataset-specific artifacts, making them less suitable for the robust, multi-dataset “all-in-one” paradigm. This validates our choice of a simpler, more robust block.

Refinement Module: We applied the same principle to the refinement block, as shown in Table 8. Our final model uses a simple “Conv” layer. We found that adding complexity, such as a “Large Conv” or a “Channel Attn.” block, unnecessarily increases the parameter count without yielding a consistent or significant performance benefit. These ablations on both the fusion and refinement modules confirm that PanTiny’s simplicity is not naive, but rather a deliberate and empirically-validated design choice that prioritizes robustness and parameter efficiency in our unified training framework.

4.4.2. Universality of the Composite Loss

To demonstrate the superiority of our loss function as a general tool, we conducted a benchmark where all competing methods were trained with it (Table 4). The pan-sharpening community has historically relied heavily on the standard

Fusion Type	Params(K)	WV2	WV3	GF2
1x1 Conv	68.2	<u>41.75</u>	<u>30.45</u>	<u>48.37</u>
Channel Attn.	71.4	41.72	30.44	48.34
Gated Conv	70.3	41.66	30.44	48.32
DeepFusion [8]	113.6	41.66	30.34	48.35
Enhanced Conv (Ours)	81.7	41.85	30.59	48.61

Table 7. Ablation on the fusion module. (Showing only PSNR).

Refine Type	Params(K)	WV2	WV3	GF2
Conv (Ours)	81.7	41.90	30.61	48.49
Channel Attn.	96.4	41.90	<u>30.55</u>	<u>48.50</u>
Large Conv	88.8	<u>41.87</u>	30.49	48.52

Table 8. Ablation on the refinement module. (Showing only PSNR).

L1 loss, often used in isolation, as it is simple and stable. However, our initial ablations in Table 6 show that using a single loss component, including L1, yields suboptimal performance.

This motivated an extensive, systematic **loss search** to find an optimal composite weighting. Our final weights ($\lambda_1 = 1.5, \lambda_2 = 4.0, \lambda_3 = 1.5$) are the result of this search, which is detailed further in our supplementary material. A key insight from this process was that while L1 provides a stable regression base, assigning a **particularly high weight to the SSIM component** ($\lambda_2 = 4.0$) consistently delivered the best performance across datasets, especially for GF2. As shown in Table 4, when competing models (often trained with a simple L1 loss in a ‘Separate’ paradigm) are retrained with our unified strategy and this optimized composite loss, they see a significant performance uplift. This demonstrates our composite loss’s power as a general tool for the community.

5. Conclusion

In this paper, we challenged the pan-sharpening community’s prevailing focus on model-centric innovation and complex cross-dataset generalization. We shifted the focus to two more practical, yet overlooked, challenges: full-resolution (FR) generalization and deployment usability. Our primary contribution is the novel “all-in-one” training paradigm, which we proved is a universally effective strategy for dramatically boosting the FR generalization (e.g., QNR) of all tested models. This paradigm also inherently solves the “one-model-per-dataset” problem, and we support this with a highly reproducible, dependency-free codebase for true usability. Finally, we proposed PanTiny, a lightweight model designed for this new paradigm. We demonstrated that this simple, efficient architecture is the SOTA performer in this practical setting, proving that principled, robust design is more effective than the complex architectural scaling seen in other works. We believe our combined contributions—the paradigm for FR generalization, the focus on usability, and the efficient PanTiny model and a universal composite loss—offer a more sustainable and practical path forward for pan-sharpening research.

References

- [1] Luciano Alparone, Bruno Aiazzi, Stefano Baronti, Andrea Garzelli, Filippo Nencini, and Massimo Selva. Multispectral and panchromatic data fusion assessment without reference. *Photogrammetric Engineering & Remote Sensing*, 74(2):193–200, 2008. 6
- [2] Zhongnan Cai, Yingying Wang, Yunlong Lin, Hui Zheng, Ge Meng, Zixu Lin, Jiabin Xie, Junbin Lu, Yue Huang, and Xinghao Ding. Pan-lut: Efficient pan-sharpening via learnable look-up tables, 2025. 7
- [3] Wjoseph Carper, Thomasm Lillesand, Ralphw Kiefer, et al. The use of intensity-hue-saturation transformations for merging spot panchromatic and multispectral image data. *Photogrammetric Engineering and remote sensing*, 56(4):459–467, 1990. 2, 4
- [4] Pierre Charbonnier, Laure Blanc-Feraud, Gilles Aubert, and Michel Barlaud. Two deterministic half-quadratic regularization algorithms for computed imaging. In *Proceedings of 1st International Conference on Image Processing*, pages 168–172. IEEE, 1994. 4
- [5] PatS. Chavez and AndyY. Kwarteng. Extracting spectral contrast in landsat thematic mapper image data using selective principal component analysis. *Photogrammetric Engineering and Remote Sensing*, 1989. 2
- [6] Wei-Ting Chen, Zhi-Kai Huang, Cheng-Che Tsai, Hao-Hsiang Yang, Jian-Jiun Ding, and Sy-Yen Kuo. Learning multiple adverse weather removal via two-stage knowledge learning and multi-contrastive regularization: Toward a unified model. In *Proceedings of the IEEE/CVF Conference on Computer Vision and Pattern Recognition*, pages 17653–17662, 2022. 1, 2
- [7] Alan R Gillespie, Anne B Kahle, and Richard E Walker. Color enhancement of highly correlated images. ii. channel ratio and “chromaticity” transformation techniques. *Remote Sensing of Environment*, page 343–365, 1987. 4
- [8] Xuanhua He, Ke Cao, Jie Zhang, Keyu Yan, Yingying Wang, Rui Li, Chengjun Xie, Danfeng Hong, and Man Zhou. Panmamba: Effective pan-sharpening with state space model. *Information Fusion*, 115:102779, 2025. 2, 3, 4, 6, 7, 8, 5
- [9] Roger L King and Jianwen Wang. A wavelet based algorithm for pan sharpening landsat 7 imagery. In *IGARSS 2001. Scanning the Present and Resolving the Future. Proceedings. IEEE 2001 International Geoscience and Remote Sensing Symposium (Cat. No. 01CH37217)*, pages 849–851. IEEE, 2001. 2
- [10] Craig A Laben and Bernard V Brower. Process for enhancing the spatial resolution of multispectral imagery using pan-sharpening, 2000. US Patent 6,011,875. 4
- [11] Xueheng Li, Tao Hu, Ke Cao, Jie Zhang, Chengjun Xie, Man Zhou, and Danfeng Hong. Pan-sharpening via causal-aware feature distribution calibration. *IEEE Transactions on Geoscience and Remote Sensing*, 63:1–14, 2025. 2, 4, 6, 7, 1
- [12] JG Liu. Smoothing filter-based intensity modulation: A spectral preserve image fusion technique for improving spatial details. *International Journal of remote sensing*, 21(18):3461–3472, 2000. 2, 4
- [13] Giuseppe Masi, Davide Cozzolino, Luisa Verdoliva, and Giuseppe Scarpa. Pansharpening by convolutional neural networks. *Remote Sensing*, 8(7):594, 2016. 1, 2, 4, 5, 6, 7
- [14] Lucien Wald. *Data fusion: definitions and architectures: fusion of images of different spatial resolutions*. Presses des MINES, 2002. 6
- [15] Jiaming Wang, Tao Lu, Xiao Huang, Ruiqian Zhang, and Xiaoxiao Feng. Pan-sharpening via conditional invertible neural network. *Information Fusion*, 101:101980, 2024. 2, 4, 5, 6, 7
- [16] Zhou Wang, Alan C Bovik, Hamid R Sheikh, and Eero P Simoncelli. Image quality assessment: from error visibility to structural similarity. *IEEE transactions on image processing*, 13(4):600–612, 2004. 5, 6, 2
- [17] Gang Yang, Xiangyong Cao, Wenzhe Xiao, Man Zhou, Aiping Liu, Xun Chen, and Deyu Meng. Panflownet: A flow-based deep network for pan-sharpening. In *Proceedings of the IEEE/CVF International Conference on Computer Vision*, pages 16857–16867, 2023. 2, 4, 5, 6, 7
- [18] Junfeng Yang, Xueyang Fu, Yuwen Hu, Yue Huang, Xinghao Ding, and John Paisley. Pannet: A deep network architecture for pan-sharpening. In *Proceedings of the IEEE international conference on computer vision*, pages 5449–5457, 2017. 1, 2, 4, 5, 6, 7
- [19] Qiangqiang Yuan, Yancong Wei, Xiangchao Meng, Huanfeng Shen, and Liangpei Zhang. A multiscale and multidepth convolutional neural network for remote sensing imagery pan-sharpening. *IEEE Journal of Selected Topics in Applied Earth Observations and Remote Sensing*, 11(3):978–989, 2018. 2, 4, 5, 6, 7

- [20] Roberta H Yuhas, Alexander FH Goetz, and Joe W Boardman. Discrimination among semi-arid landscape endmembers using the spectral angle mapper (sam) algorithm. In *JPL, Summaries of the Third Annual JPL Airborne Geoscience Workshop. Volume 1: AVIRIS Workshop*, 1992. 6
- [21] Jie Zhang, Ke Cao, Keyu Yan, Yunlong Lin, Xuanhua He, Yingying Wang, Rui Li, Chengjun Xie, Jun Zhang, and Man Zhou. Frequency decoupled domain-irrelevant feature learning for pan-sharpening. *IEEE Transactions on Circuits and Systems for Video Technology*, 2024. 2

Rethinking Pan-sharpening: A New Training Process for Full-Resolution Generalization

Supplementary Material

6. On the Limitations of Generalization and the Necessity of All-in-One Training

In the main paper, we argue that our “all-in-one” training paradigm is a superior approach to achieving robust pan-sharpening models compared to existing generalization methods. Here, we provide detailed experimental evidence to support this claim. The conventional approach to generalization—training a model on a single source dataset and testing it on multiple unseen target datasets—often fails to bridge the significant domain gap between different satellite sensors. We contend that this approach often leads to models that are merely overfitted to the source domain, rather than being truly generalizable.

6.1. The Challenge of Domain Gaps in Pan-sharpening Datasets

A fundamental challenge in pan-sharpening is the significant domain gap between datasets from different satellite sensors. For instance, the datasets used in our study—WorldView-2 (WV2), WorldView-3 (WV3), and GaoFen-2 (GF2)—exhibit substantial differences. WV2 and WV3 provide 8-band multispectral images, which are conventionally processed down to 4 bands for standard pan-sharpening tasks, whereas GF2 directly provides 4-band data. Furthermore, these satellites operate with different sensors, at different altitudes, and capture images with varying ground resolutions and atmospheric conditions. This inherent data heterogeneity means that a model optimized for one dataset’s specific spectral and spatial characteristics will inevitably struggle to perform well on another. This large domain gap makes true generalization exceptionally difficult and underscores the limitations of single-dataset training.

6.2. The “One-Epoch Generalization” Illusion

To test the hypothesis of overfitting in conventional generalization studies, we conducted a surprising experiment: we trained several of our intermediate models for only **one epoch** on the WV2 dataset and then evaluated their performance on the unseen WV3 and GF2 datasets. The results, shown in Table 10, are striking. When tested on GF2, our one-epoch trained “M4 (Channel Attn)” model achieves a PSNR of 39.13. This result is comparable to or even surpasses the performance of fully-trained models from dedicated generalization papers, such as DDIF [6], which reports a PSNR of 37.77 on GF2 after being fully trained on WV2 (see Table 9). This suggests that the hundreds of addi-

tional training epochs in those works contribute little to true generalization, instead primarily reinforcing the model’s bias towards the source dataset. This finding strongly motivates a shift away from the “train-on-one, test-on-many” methodology. Any reviewer can easily verify this conclusion with a personal computer in under 5 minutes using our provided codebase, if they already have the datasets.

6.3. The Overfitting Trap of Separate Training

Further evidence against the separate training paradigm comes from analyzing the cross-domain performance of our own model when fully trained on a single dataset. Table 11 shows the results of training “PanTiny (Big)” to convergence on one source dataset and testing on all three. For instance, the model trained on WV2 achieves an excellent 42.16 PSNR on its own test set, but its performance plummets to 21.76 on WV3 and 33.92 on GF2. This performance is substantially worse than the one-epoch results, proving that prolonged training on a single dataset actively harms its ability to generalize by causing it to overfit to the source domain’s specific characteristics.

6.4. Failure Case: Generalization to Jilin-1 Dataset

To push the boundaries of generalization, we tested our all-in-one trained models on the Jilin-1 dataset, which was completely unseen during training. As shown in Table 12, the performance of all models is poor, indicating that even our robust “all-in-one” paradigm has its limits when faced with a significant domain shift. Interestingly, PSCINN, which performed poorly on the training datasets, shows relatively better (though still low) performance here, possibly due to its different architectural inductive biases. This experiment reinforces our central thesis: true generalization in pan-sharpening is a data problem, and robust performance requires training on diverse, representative datasets.

7. Detailed Ablation on the Composite Loss

7.1. The Overlooked Potential of Loss Functions

Historically, the pan-sharpening community has predominantly focused on advancing model architectures to achieve performance gains. The L1 loss has long been the de-facto standard, with the majority of research efforts dedicated to designing more sophisticated networks. However, this model-centric approach appears to be reaching a point of diminishing returns. As evidenced by recent SOTA models like CFDCNet [11], achieving marginal performance im-

Method	WorldView-III			Worldview-II			GaoFen2		
	PSNR↑	SSIM↑	SAM↓	PSNR↑	SSIM↑	SAM↓	PSNR↑	SSIM↑	SAM↓
PNN	21.9204	0.5771	0.1301	40.8487	0.9642	0.0254	28.6188	0.8649	0.1177
PANNET	22.3157	0.5597	0.1273	40.8176	0.9626	0.0257	35.0812	0.8707	0.0422
MSDCNN	21.2841	0.5651	0.1551	41.3355	0.9664	0.0242	29.6255	0.8815	0.1062
DICNN	19.1958	0.5606	0.1453	39.9554	0.9597	0.0275	34.4568	<u>0.8857</u>	0.0447
SRPPNN	22.0543	0.5779	0.1340	41.4538	0.9679	0.0233	33.7282	0.7989	0.0513
Panformer	19.3288	0.5715	0.1533	41.2170	0.9672	0.0239	23.4309	0.8192	0.2239
Mutual	21.7467	0.5783	0.1488	41.6773	0.9705	0.0224	34.0899	0.8380	0.0523
LAGConv	21.6249	0.5520	0.1516	41.6815	0.9598	0.0325	35.1923	0.8753	0.0436
SFIIN	21.9983	0.5766	0.1310	41.7080	0.9693	0.0228	<u>36.7285</u>	0.8705	<u>0.0307</u>
P2Net	<u>22.4445</u>	<u>0.6084</u>	<u>0.1258</u>	41.9229	<u>0.9711</u>	<u>0.0219</u>	35.4512	0.8383	0.0386
DDIF	22.9937	0.6102	0.1213	<u>41.7219</u>	0.9719	0.0217	37.7663	0.8919	0.0253

Table 9. Quantitative comparison from a prior generalization work [6], with the model trained on the Worldview-II dataset and tested on other datasets. The best results are marked in **bold** and the second results are marked with underline. ↑ indicates that the larger the value, the better the performance, and ↓ indicates that the smaller the value, the better the performance.

Model	Params(K)	FLOPs(G)	WV2			WV3			GF2		
			PSNR↑	SSIM↑	SAM↓	PSNR↑	SSIM↑	SAM↓	PSNR↑	SSIM↑	SAM↓
M3 (Dual Enc.)	128.9	4.22	38.00	0.9347	0.0352	22.12	0.5608	0.1272	35.90	0.9227	0.0378
pantiny(small) (Single Enc.)	48.3	1.58	36.38	0.9127	0.0396	22.05	0.5352	0.1317	34.39	0.9230	0.0627
M4 (Gated Conv)	67.0	2.20	36.84	0.9195	0.0358	22.09	0.5668	0.1264	37.67	0.9450	0.0297
M4 (Channel Attn)	66.0	2.16	36.87	0.9174	0.0358	22.34	0.5710	0.1243	39.13	0.9263	0.0260

Table 10. Performance of various intermediate models after only **one epoch** of training on the WV2 dataset, tested on all three datasets. The competitive results on unseen domains (WV3, GF2) challenge the effectiveness of conventional generalization strategies.

Training Dataset	Test on WV2			Test on WV3			Test on GF2		
	PSNR↑	SSIM↑	SAM↓	PSNR↑	SSIM↑	SAM↓	PSNR↑	SSIM↑	SAM↓
WV2 Only	42.16	0.9711	0.0217	21.76	0.5628	0.1284	33.92	0.8899	0.0433
WV3 Only	27.99	0.7880	0.0964	30.61	0.9245	0.0747	24.75	0.6798	0.0863
GF2 Only	34.40	0.8882	0.0438	21.89	0.4650	0.1279	48.93	0.9900	0.0092

Table 11. Cross-domain performance of “PanTiny (Big)” when trained separately on a single source dataset. The drastic performance drop on target datasets highlights the overfitting issue inherent in this paradigm.

provements now requires an enormous increase in computational cost (over 55G FLOPs), suggesting an architectural bottleneck.

We posit that the loss function, a relatively underexplored area, holds the key to unlocking the next level of performance. While perceptual losses like SSIM [16] have been considered, they were often dismissed after preliminary tests showed that using them in isolation or with balanced weights did not yield superior results and could sometimes introduce color artifacts. This led to a widespread underestimation of their potential. We believe that a system-

atic, large-scale exploration of loss combinations has been a missing piece in the field.

7.2. Our Systematic Two-Stage Search for the Optimal Loss

Our work is the first, to our knowledge, to conduct such an extensive search. This process, detailed in Table 13, was divided into two stages.

In the first stage, we conducted a broad search using our “PanTiny (Big)” model to understand the general behavior of different loss component weightings. We tested balanced

Model	Jilin-1		
	PSNR \uparrow	SSIM \uparrow	SAM \downarrow
PNN	22.16	0.6000	0.1286
PanNet	22.82	<u>0.6255</u>	0.0911
PanFlow	22.14	0.5641	<u>0.0861</u>
MSDCNN	21.73	0.5988	0.1321
PSCINN	27.90	0.8319	0.0812
Ours (PanTiny Big)	<u>23.10</u>	0.5694	0.0884

Table 12. Zero-shot generalization performance on the unseen Jilin-1 dataset. All models were trained under the “all-in-one” paradigm. The best results are in **bold** and the second results are marked with underline.

configurations like (1,1,1) as well as configurations focusing on each individual component. This initial exploration yielded a crucial insight: combinations with a high weight on the SSIM component, such as (1,3,1), consistently outperformed others.

Guided by this finding, we initiated a second, more fine-grained search stage. To accelerate experimentation, we used our lighter “PanTiny (Small)” model and focused exclusively on high-SSIM weight combinations. This meticulous process allowed us to identify the “(1.5, 4.0, 1.5)” configuration as the most robust and highest-performing combination. This discovery is not just a set of tuned hyper-parameters; it represents a universally applicable principle that can elevate the entire field. By applying this composite loss, we have unlocked a new tier of performance, pushing the SOTA for metrics like GF2 PSNR into the 48-49 dB era for a wide range of models.

8. Detailed Ablation on Model Architecture

Our final PanTiny architecture was the result of a systematic exploration of different design choices, moving from complex structures to a refined, efficient final model. Our initial explorations included models with multiple downsampling levels and dual-encoder designs (named M3, M4, M5), but these were ultimately superseded by the more efficient single-encoder architecture of PanTiny.

8.1. Downsampling Strategy

A common strategy in image restoration is to use a U-Net-like architecture with multiple downsampling stages to capture multi-scale features. We investigated this by creating variants of our base model (“PanTiny(Small)”) with 0, 2, and 4 downsampling levels, using a basic L1 loss for a fair architectural comparison. As shown in Table 14, we found that increasing the downsampling levels led to a significant increase in parameters and a decrease in overall performance. The 0-level model (no downsampling) performed the best, indicating that for pan-sharpening, maintaining the

full feature resolution is more effective. This led us to adopt a flat, single-scale architecture for PanTiny.

8.2. Investigating the “DeepFusion” Module

In our main paper, we noted that Pan-Mamba’s performance degrades significantly in the “all-in-one” setting. We hypothesized this was due to its complex “DeepFusion” module overfitting to single-dataset characteristics. To verify this, we integrated the “DeepFusion” block into our “m6” experimental model. As shown in Table 15, not only does the “DeepFusion” block increase parameter count, but it also consistently underperforms compared to simpler fusion mechanisms like our “Enhanced Conv” (from the main paper’s ablation) or even basic “Gated Conv” and “Channel Attention”. Furthermore, increasing the depth of the “DeepFusion” block from 2 to 5 layers leads to a further drop in performance. This provides strong evidence that such complex fusion modules, while effective for a single dataset, are detrimental to generalization in the “all-in-one” paradigm.

8.3. Single-Encoder vs. Dual-Encoder Design

In our architectural exploration, we also compared single-encoder and dual-encoder designs. Our “m5” model variant features a dual-encoder architecture, while “m6” uses a single encoder. Table 16 presents a controlled comparison where both models use a channel attention fusion mechanism. The “m6” model, despite having significantly fewer parameters (64.3K vs. 118.5K), consistently outperforms the larger dual-encoder “m5” model. This result was pivotal, leading us to abandon the more complex dual-encoder structure. We concluded that allocating parameters towards a more effective fusion and body in a single-encoder framework provides a better performance-efficiency trade-off, which became a core principle in designing the final “PanTiny” model.

8.4. Full Ablation Results for Final Model Components

The main paper presented condensed versions of our final fusion and refinement ablations for brevity. Here, we provide the complete tables with all metrics (Table 17 and Table 18). These results reinforce our conclusion that for “PanTiny”, simple and well-chosen convolutional blocks outperform more complex alternatives in the multi-dataset setting, providing the best balance of parameter efficiency and performance.

9. Additional Visual Results

To save space in the main paper, we presented a limited set of visual comparisons. This section provides additional qualitative examples to complement the quantitative results. These examples offer a more intuitive understanding of the performance differences between various methods across

Loss Combination (L1, SSIM, Focal)	Model	WV2			WV3			GF2		
		PSNR↑	SSIM↑	SAM↓	PSNR↑	SSIM↑	SAM↓	PSNR↑	SSIM↑	SAM↓
<i>Stage 1: Broad Search on PanTiny (Big)</i>										
L1 only (1.0, 0, 0)	pantiny	39.77	0.9532	0.0285	29.19	0.8939	0.0953	45.42	0.9782	0.0141
SSIM only (0, 1.0, 0)	pantiny	40.82	0.9648	0.0254	29.91	0.9158	0.0816	47.21	0.9865	0.0111
Focal only (0, 0, 1.0)	pantiny	39.87	0.9545	0.0281	29.18	0.8937	0.0933	44.80	0.9757	0.0150
Balanced (0.8, 0.5, 0.4)	pantiny	41.00	0.9640	0.0248	29.99	0.9128	0.0832	47.38	0.9859	0.0110
Equal (1.0, 1.0, 1.0)	pantiny	41.28	0.9659	0.0240	30.17	0.9170	0.0791	47.68	0.9869	0.0105
SSIM Focus (1.0, 3.0, 1.0)	pantiny	41.57	0.9680	0.0232	30.37	0.9213	0.0771	48.14	0.9882	0.0100
L1 Focus (3.0, 1.0, 1.0)	pantiny	41.38	0.9663	0.0237	<u>30.31</u>	<u>0.9186</u>	<u>0.0777</u>	<u>47.99</u>	<u>0.9877</u>	<u>0.0102</u>
Focal Focus (1.0, 1.0, 3.0)	pantiny	<u>41.41</u>	<u>0.9665</u>	<u>0.0236</u>	30.28	0.9177	<u>0.0777</u>	47.92	0.9875	<u>0.0102</u>
<i>Stage 2: Fine-grained Search on PanTiny (Small)</i>										
(2.0, 2.0, 2.0)	panrestormer	41.60	0.9680	0.0231	30.38	0.9206	0.0768	48.17	0.9884	<u>0.0099</u>
(3.0, 0.8, 1.0)	panrestormer	41.32	0.9661	0.0237	30.30	0.9180	0.0777	47.95	0.9876	0.0102
(0.8, 0.8, 3.0)	panrestormer	41.35	0.9664	0.0237	30.27	0.9177	0.0779	48.13	0.9880	<u>0.0099</u>
(0.8, 5.0, 1.0)	panrestormer	41.66	<u>0.9689</u>	0.0228	30.40	<u>0.9227</u>	0.0767	48.25	0.9887	<u>0.0099</u>
(1.5, 3.5, 1.5)	panrestormer	41.64	0.9686	<u>0.0229</u>	30.42	0.9219	0.0765	<u>48.28</u>	<u>0.9886</u>	0.0098
(0.8, 3.0, 1.0)	panrestormer	41.52	0.9681	0.0232	30.39	0.9213	0.0768	48.06	0.9883	0.0101
(0.5, 8.0, 0.5)	panrestormer	<u>41.68</u>	0.9694	0.0228	<u>30.45</u>	0.9233	0.0760	48.17	0.9887	0.0100
(1.5, 4.0, 1.5)	panrestormer	41.70	<u>0.9689</u>	0.0228	30.46	0.9225	<u>0.0761</u>	48.29	0.9887	0.0098

Table 13. Full ablation study on loss function components and weights. The top part shows a broad search on our “PanTiny (Big)” model, while the bottom part shows a fine-grained search on the “PanTiny (Small)” model to accelerate experiments. Our proposed combination (1.5, 4.0, 1.5) provides the best overall performance. Best results are in **bold**, second-best are underlined.

Model	Params(K)	FLOPs(G)	WV2			WV3			GF2		
			PSNR↑	SSIM↑	SAM↓	PSNR↑	SSIM↑	SAM↓	PSNR↑	SSIM↑	SAM↓
4-ds	446.7	14.64	39.59	0.9543	0.0287	<u>28.93</u>	0.8926	0.0977	45.33	0.9791	<u>0.0140</u>
2-ds	121.2	3.97	40.74	0.9627	0.0255	29.58	<u>0.9079</u>	<u>0.0856</u>	46.74	0.9840	0.0118
0-ds (Ours)	48.0	1.57	<u>40.58</u>	<u>0.9618</u>	<u>0.0257</u>	29.58	0.9083	0.0849	<u>46.64</u>	<u>0.9839</u>	0.0118

Table 14. Ablation on downsampling levels using a simple L1 loss. Deeper U-Net-like structures did not improve performance. Best results are in **bold**, second-best are underlined.

Fusion Type	Params(K)	WV2			WV3			GF2		
		PSNR↑	SSIM↑	SAM↓	PSNR↑	SSIM↑	SAM↓	PSNR↑	SSIM↑	SAM↓
Gated Conv	63.2	<u>40.95</u>	<u>0.9639</u>	0.0248	30.04	0.9149	0.0800	<u>47.37</u>	<u>0.9860</u>	0.0108
Channel Attention	64.3	41.06	0.9641	0.0248	<u>30.00</u>	<u>0.9133</u>	0.0830	47.54	0.9864	0.0108
DeepFusion (2 layers)	75.2	40.78	0.9625	<u>0.0254</u>	29.88	0.9127	<u>0.0822</u>	46.99	0.9851	<u>0.0113</u>
DeepFusion (5 layers)	106.5	40.67	0.9625	0.0255	29.87	0.9122	0.0823	46.87	0.9848	0.0116

Table 15. Ablation on the “DeepFusion” module using our “m6” variant. Complex, deep fusion strategies underperform simpler ones in the multi-dataset setting.

Model (Encoder Type)	Params(K)	WV2			WV3			GF2		
		PSNR↑	SSIM↑	SAM↓	PSNR↑	SSIM↑	SAM↓	PSNR↑	SSIM↑	SAM↓
m5 (Dual-Encoder, Large)	118.5	41.05	0.9642	0.0246	29.89	0.9119	0.0842	47.45	0.9860	0.0109
m6 (Single-Encoder)	64.3	41.06	0.9641	0.0248	30.00	0.9133	0.0830	47.54	0.9864	0.0108

Table 16. Comparison between our single-encoder (“m6”) and dual-encoder (“m5”) experimental models. The single-encoder design achieves superior performance with fewer parameters.

Fusion Type	Params (K)	WV2			WV3			GF2		
		PSNR \uparrow	SSIM \uparrow	SAM \downarrow	PSNR \uparrow	SSIM \uparrow	SAM \downarrow	PSNR \uparrow	SSIM \uparrow	SAM \downarrow
1x1 Conv	68.2	<u>41.75</u>	<u>0.9690</u>	<u>0.0227</u>	<u>30.45</u>	<u>0.9222</u>	<u>0.0761</u>	<u>48.37</u>	<u>0.9888</u>	<u>0.0098</u>
Channel Attn.	71.4	41.72	0.9686	0.0228	30.44	0.9216	0.0767	48.34	0.9886	<u>0.0097</u>
Gated Conv	70.3	41.66	0.9686	0.0229	30.44	0.9219	0.0766	48.32	0.9886	<u>0.0098</u>
DeepFusion [8]	113.6	41.66	0.9684	0.0229	30.34	0.9206	0.0771	48.35	0.9887	<u>0.0098</u>
Enhanced Conv (Ours)	81.7	41.85	0.9696	0.0224	30.59	0.9238	0.0749	48.61	0.9894	0.0095

Table 17. Full ablation results for the fusion module in the final ‘PanTiny’ architecture. Our ‘Enhanced Conv’ provides the best overall trade-off.

Refine Type	Params (K)	WV2			WV3			GF2		
		PSNR \uparrow	SSIM \uparrow	SAM \downarrow	PSNR \uparrow	SSIM \uparrow	SAM \downarrow	PSNR \uparrow	SSIM \uparrow	SAM \downarrow
Conv (Ours)	81.7	41.90	<u>0.9697</u>	<u>0.0224</u>	30.61	0.9240	0.0749	48.49	0.9891	0.0097
Channel Attn.	96.4	41.90	0.9698	0.0223	30.55	<u>0.9230</u>	<u>0.0751</u>	48.50	0.9891	0.0096
Large Conv	88.8	<u>41.87</u>	0.9696	<u>0.0224</u>	30.49	0.9225	0.0759	48.52	0.9891	0.0096

Table 18. Full ablation results for the refinement module in the final ‘PanTiny’ architecture. A simple convolution is most effective.

all three datasets (WV2, WV3, and GF2) and demonstrate the robustness of our approach.

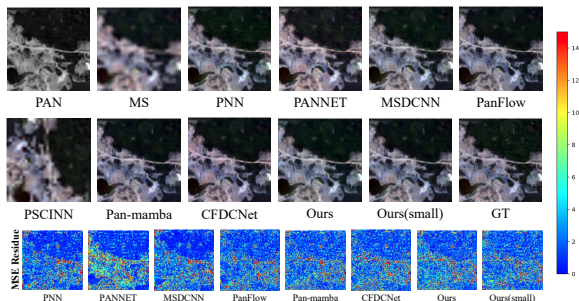


Figure 5. Visual comparison on the WorldView-2 (WV2) dataset.

10. Codebase and Reproducibility

To ensure full reproducibility and facilitate future research, we provide a comprehensive and easy-to-use codebase as a ‘code.tar.gz’ archive in the supplementary materials. Our framework is built around a unified experiment runner that leverages a hierarchical YAML configuration system. This allows researchers to define a base configuration and then specify a series of experiments that inherit and override these settings, enabling efficient and organized ablation studies. For more details, please refer to the ‘README.md’ file included in our supplementary materials.

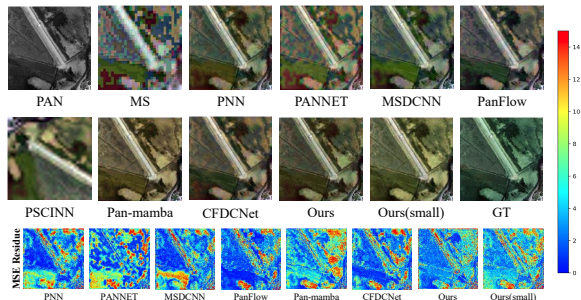


Figure 6. Visual comparison on the WorldView-3 (WV3) dataset. Our method performs exceptionally well when the multispectral (MS) image contains a significant amount of noise.

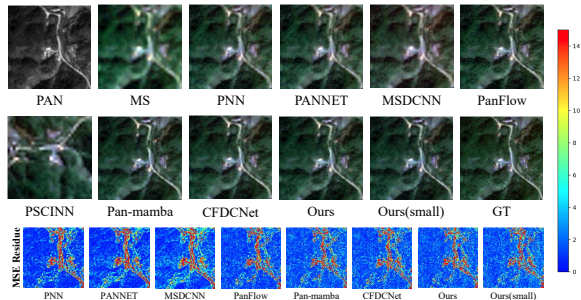


Figure 7. Visual comparison on the GaoFen-2 (GF2) dataset.